Reporter Review: Inner magnetosphere

Yusuke Ebihara
Institute for Advanced Research, Nagoya University, Japan

- The purpose of this review is to summarize the consequences of the inner magnetospheric processes, including
  - Plasmasphere, warm plasma, ring current, radiation belt, and subauroral phenomena.
- At least 221 papers were published in this area in the last 2 years, as far as I surveyed.
- The time is limited. Please forgive me for not fully reviewing all the papers.

Outline

- Plasmasphere
- Warm plasma
- Ring current
- Radiation belt
- Sawtooth event
- Ionosphere coupling: SAPS/SAID
- Ionosphere coupling: Aurora
- Summary

Plasmasphere

Global view of plasmaspheric refilling

- First global imaging of the plasmaspheric refilling.
  - At 0 h, convection eroded the plasmasphere so that the plasmapause is sharply defined near L ~ 3–4.
  - At 28 h, the plasmasphere has expanded, its interior is structured in azimuth, and the plasmapause is diffuse.
  - At 69 h, the plasmapause lies outside L = 6 and the interior is less structured in azimuth.
- Averaged volume refilling rates are
  - ~1 cm^{-3} h^{-1} at L = 3.3
  - ~7×10^{-2} cm^{-3} h^{-1} at L = 6.3

  which are generally consistent with earlier, more local measurements.

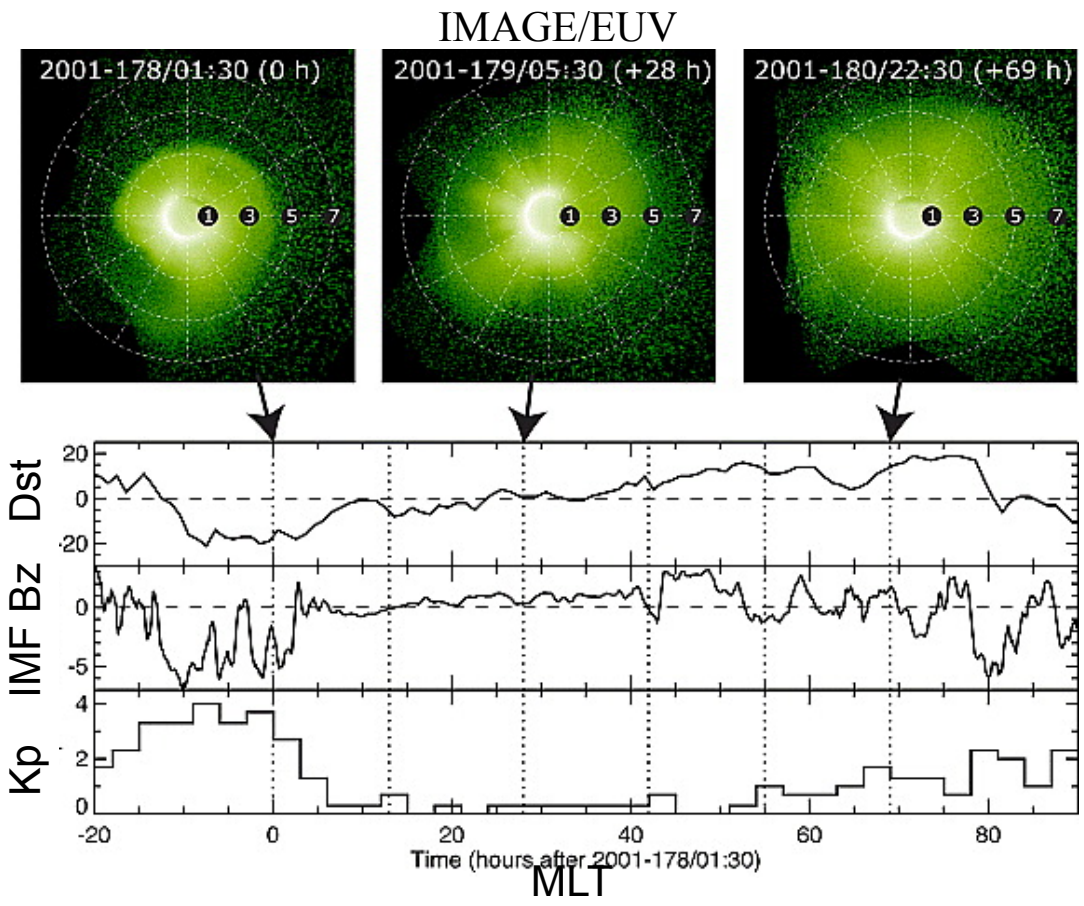

Sandel and Denton (2007, GRL)

Diurnal variation of plasmaspohere

- Diurnal variation of the He^+ density in the core plasmasphere at L=2.5 was found.
- No significant dependence on geomagnetic activity is shown.
- He^+ density increases soon after dawn, decreases or stagnates around noon, and strongly increase in late afternoon.
  - Diurnal refilling is largely controlled by photoionization.
  - Increase in He^+ at dusk is attributed to north-south asymmetry of ionospheric condition, or bulge effect.

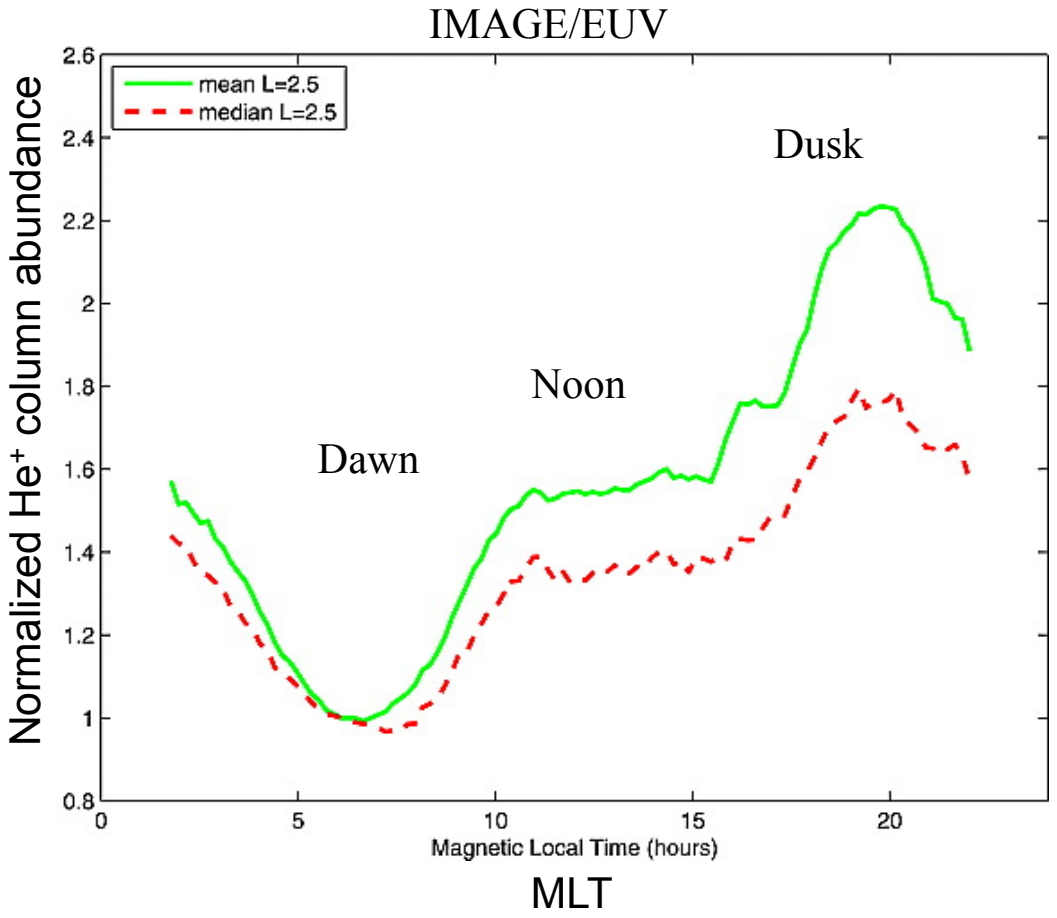

Galvan et al. (2008, JGR)

Plasmapause identification from DMSP

- Method (7 steps) for extracting the ionospheric projection of the plasmapause from DMSP of H^+ density was developed (Anderson et al., 2008, GRL).

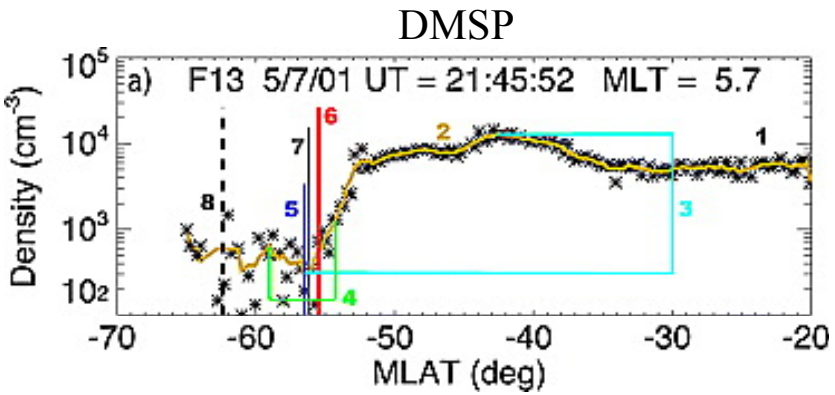

H^+ density measurements from the DMSP . The red vertical line indicates the identified plasma pause location. The numbers 1–7 refer to the steps of the PP identification procedure

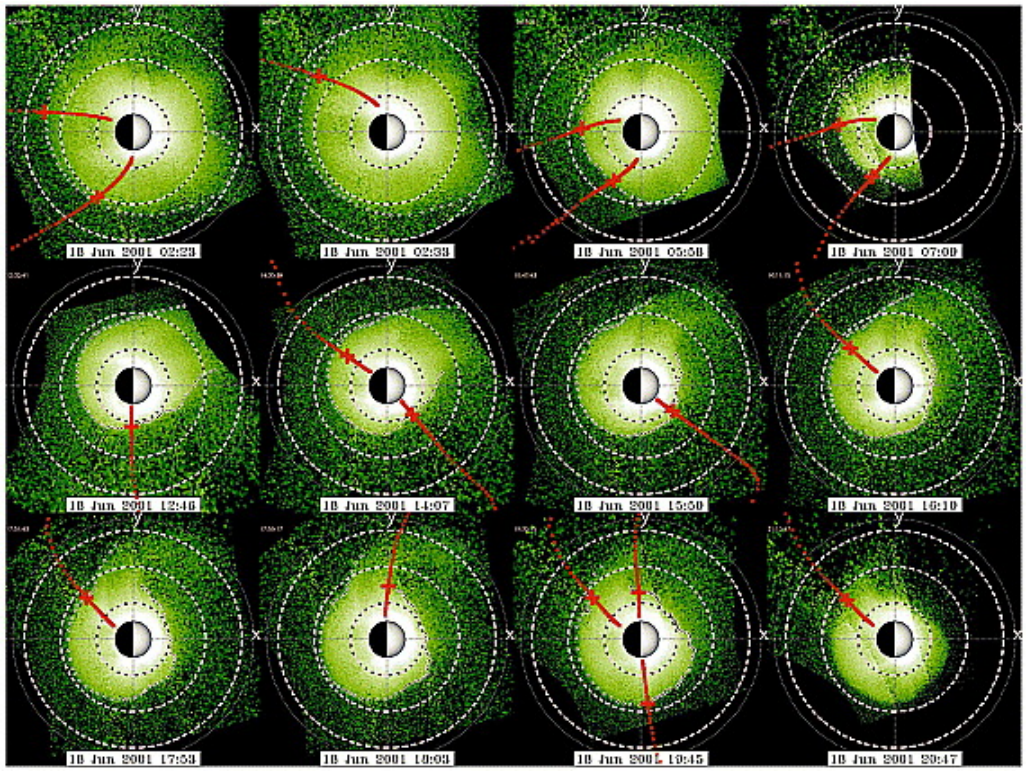

IMAGE EUV observations of the plasmaspheric He^+ density. Each panel shows the He^+ distribution in the equatorial plane. The Sun is to the right. The red traces show DMSP orbit tracks mapped to the equatorial plane. The red crosses indicate the location of the ionospheric projection of the DMSP-inferred plasmapause, which is consistent with the IMAGE EUV observation.

Anderson et al. (2008, GRL)

Plasmaspheric drainage plumes

- Plasmaspheric cold ions are transferred sunward at typically 2×10^{26} ions/sec (1.2 ton/hr of protons) via the plasmaspheric plume (Borovsky and Denton, 2008, JGR).
  - A total of approximately 2×10^{31} ions (34 tons of protons) are transported in the life of a storm.

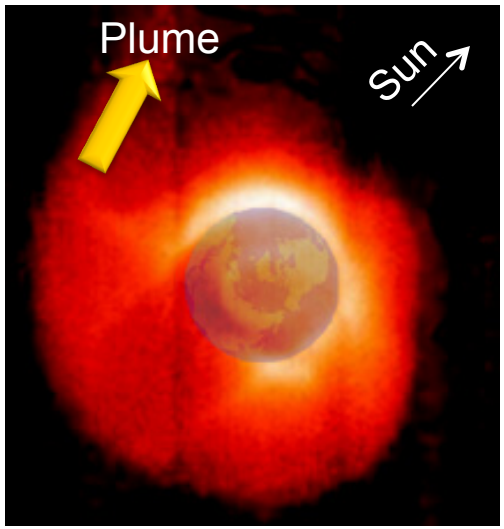

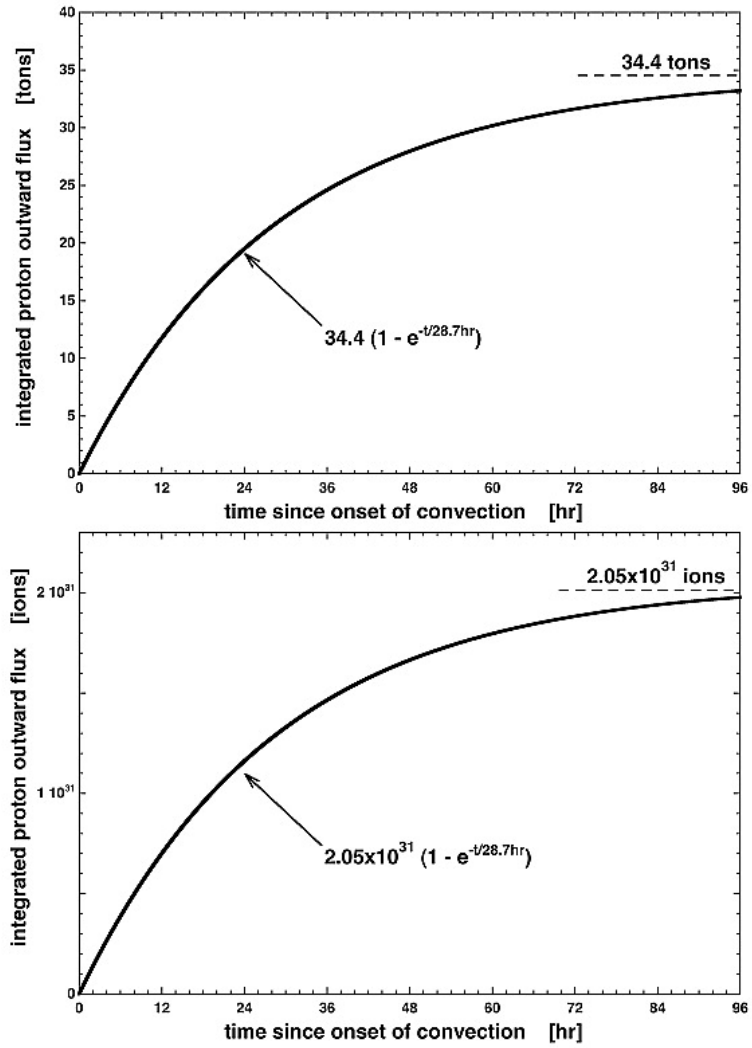

Time integrals of the exponential fits to the measured total ion fluxes are plotted as functions of time. In the top, the units are ions, and in the bottom, the units are tons of protons.

Borovsky and Denton (2008, JGR)

Plasmaspheric plume participating in reconnection

- Dense plasmaspheric plume extends to the magnetopause, and participates in reconnection (McFadden et al., 2008, GRL).
  - At the magnetopause, cold ions and reconnection flow jets coexist on open flux tubes.

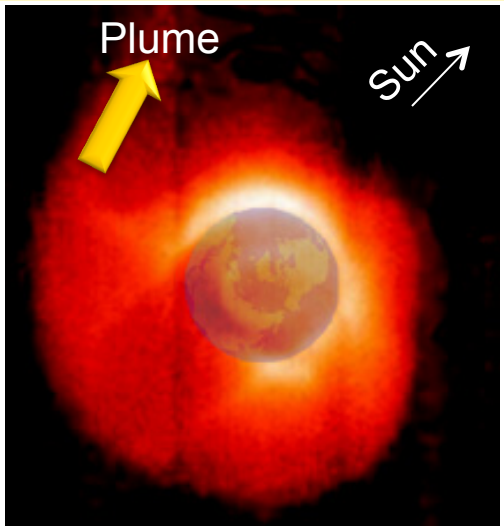

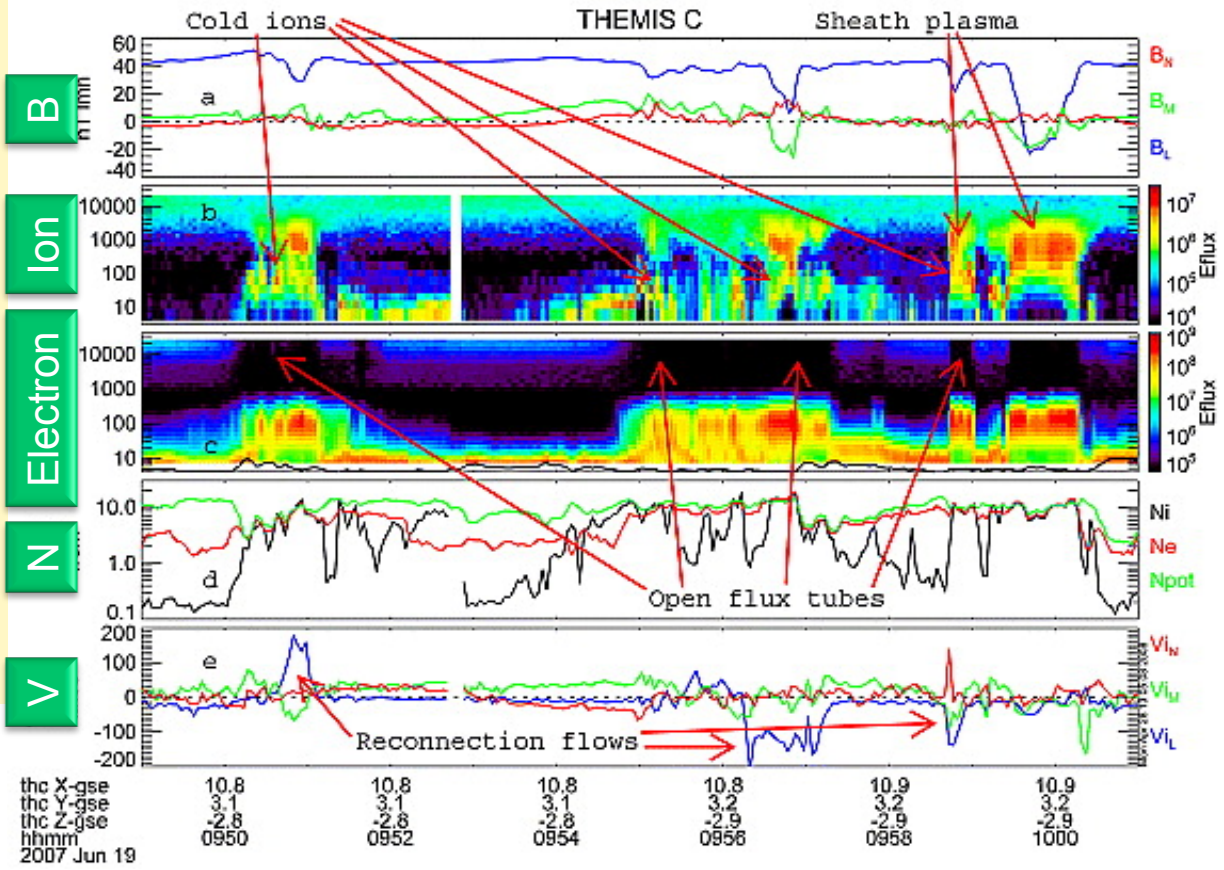

For the THC probe, (a) magnetic field, (b) ion and (c) electron spectrograms, (d) density, and (e) ion velocity during several encounters with the magnetopause. The cold plasma dominated magnetosphere has about the same density as the magnetosheath. Cold ions (spectral peak <200 eV in Figure 3b) are observed on newly reconnected field lines during the periods 0950–0951 UT, 0955–0957 UT, and just before 0959 UT. Reconnection is determined from the loss of hot electrons and from reconnection flow jets.

McFadden et al. (2008, GRL)

Plasmaspheric wind

- Plasmaspheric plume supplies ions to the entire region of the magnetosphere.
- Re-circulation of ions are possible.

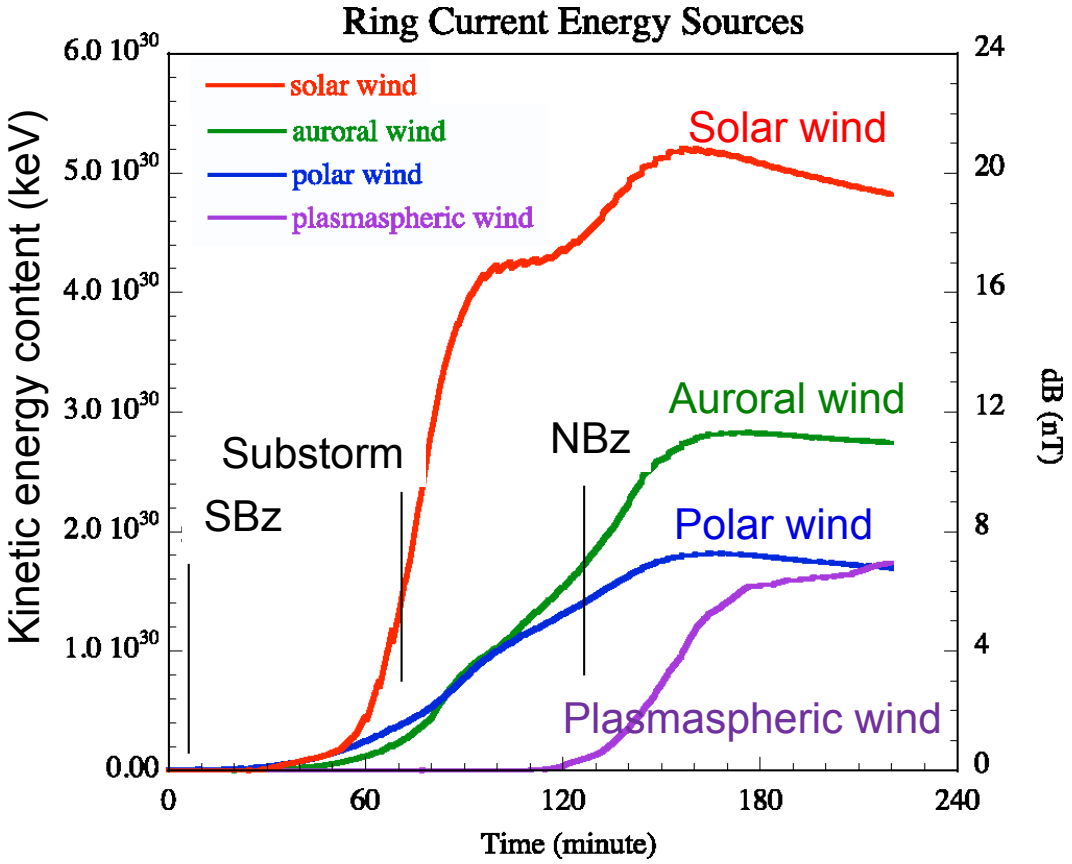

Inner magnetosphere kinetic energy content development during the simulation for the four sources considered.

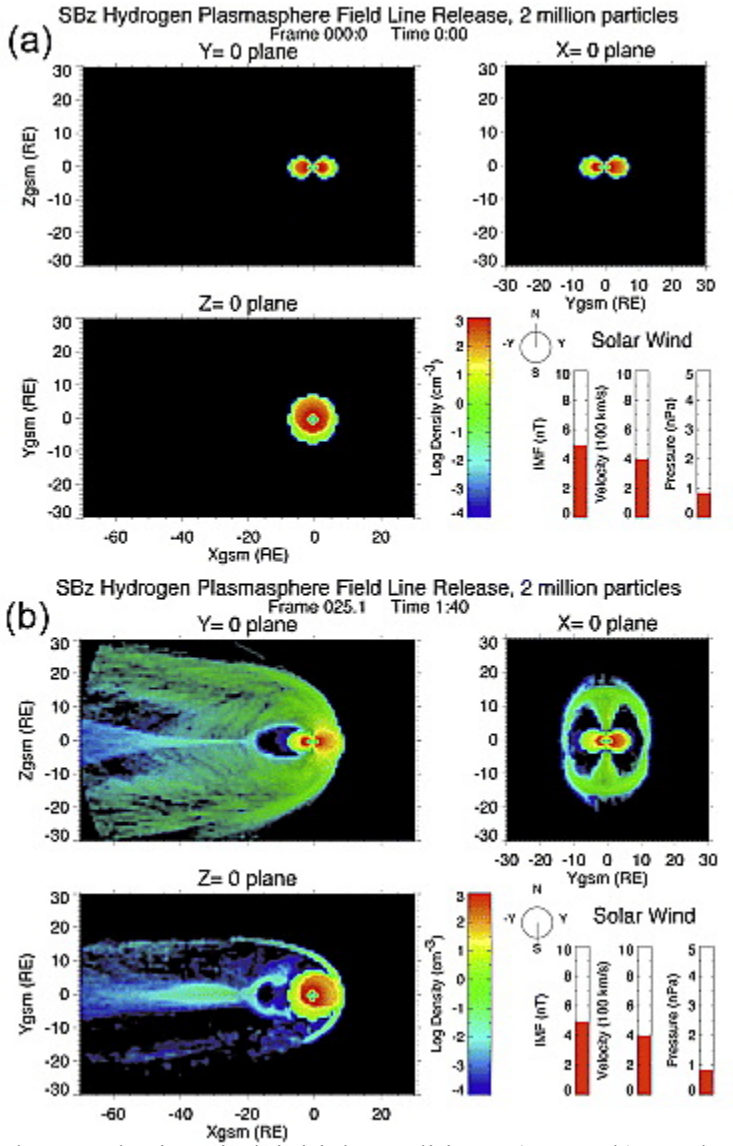

(a) The plasmaspheric wind initial conditions (00:00 h), and the response to southward IMF, with (b) resultant day and night side reconnection (01:40 h).

Moore et al. (2008, JGR)

Warm plasma

Warm plasma cloak

- Warm plasma (~a few eV – several hundred eV) is prominent on the dawn side.
  - Bi-directional field-aligned pitch angle distribution.
  - Not categorized into plasmasphere, ring current and radiation belt.
- This can be explained in terms of drift trajectories depending on energy.
- Ionospheric ions reach the magnetotail. After energized, the ion tends to drift eastward if the energy is < 3 keV. The ion will drift westward if energy is > 3keV.

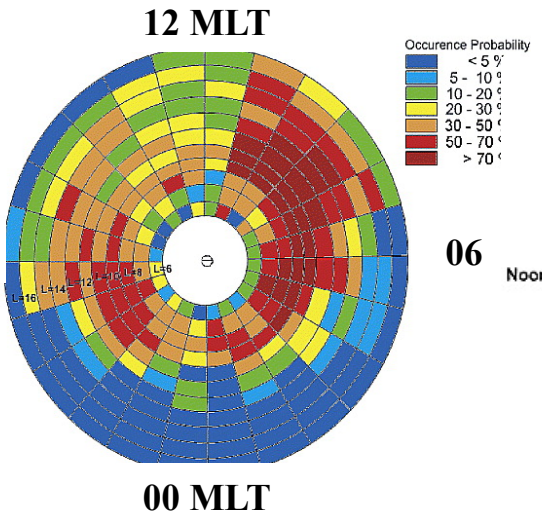

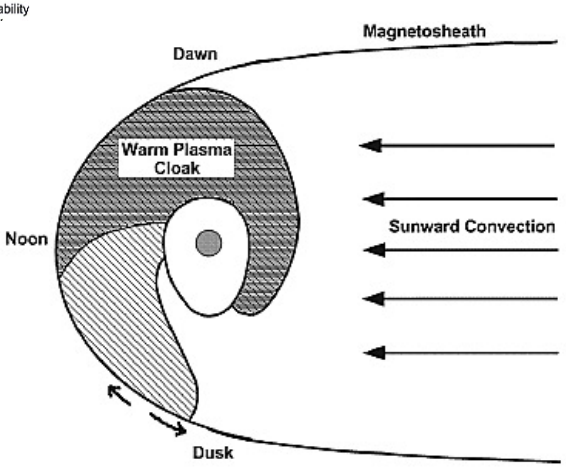

Occurrence probability of low-energy (less than 400 eV) bidirectional field-aligned distributions plotted in local time versus L shell. Calculations are based on TIDE/Polar.

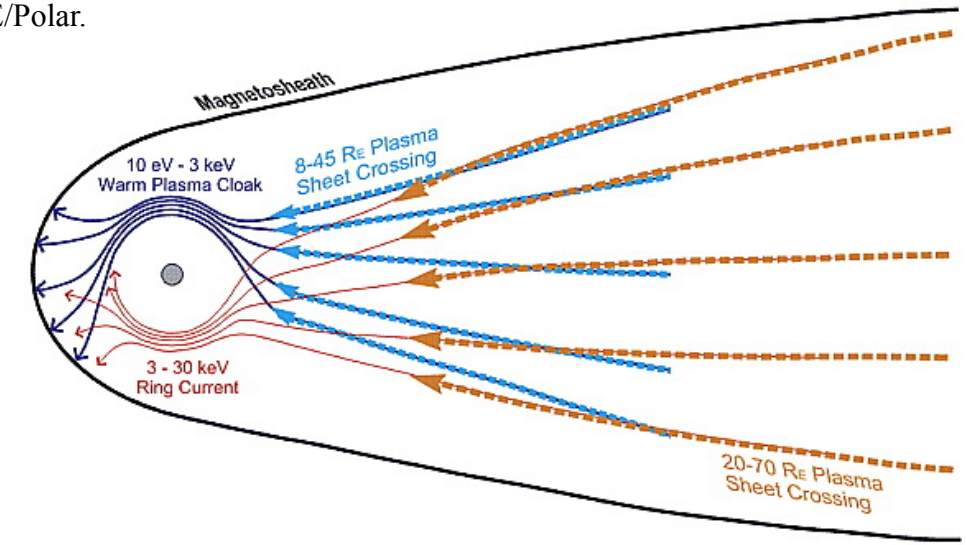

Chappell et al. (2008, JGR)

Warm ions

- Warm ions exhibit small-scale stripes with energy-*L* dispersion. This is called (partial) wedge-like dispersion.
- Temperature of the warm ions is <100 eV, which is distinguished from the ring current and the plasma sheet.
- They appear outside of the typical plasmapause location. Thus, they come from the magnetotail under the influence of the convection.
- Because the temperature is different from the ring current and the plasma sheet, warm ions cannot be understood to the transportation of ions.
- Origin of the small-scale stripes is unknown.

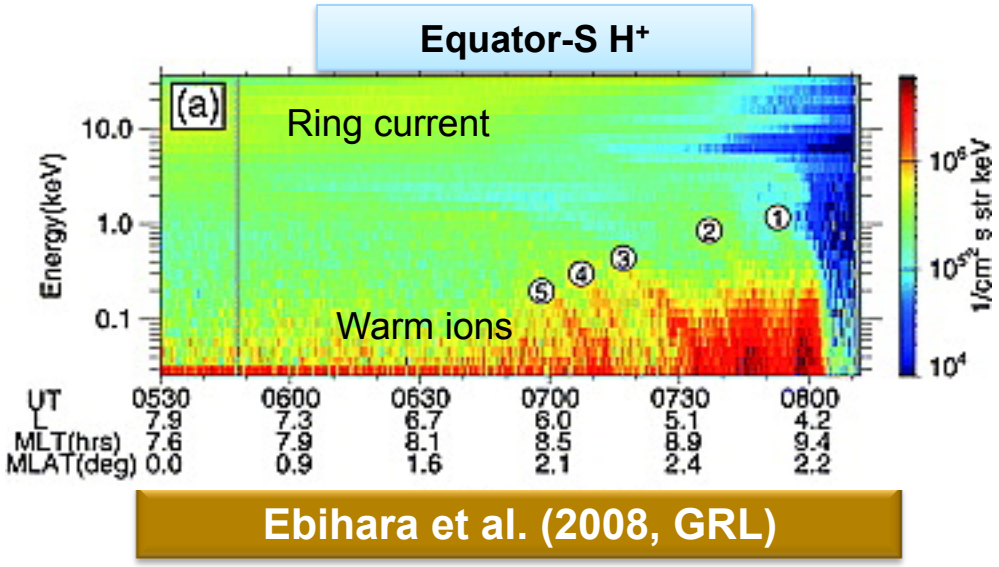

Ebihara et al. (2008, GRL)

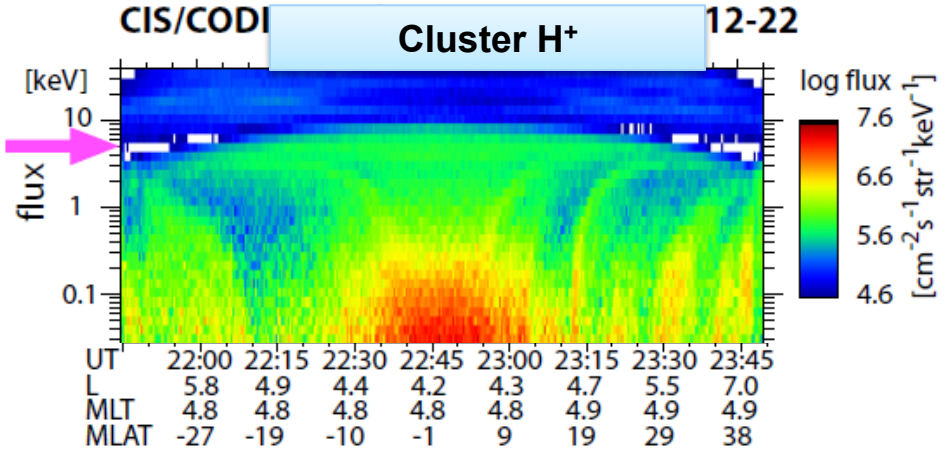

Yamauchi et al. (2009, AG.)

Warm (suprathermal) electrons

- Warm (suprathermal) electrons appear on the dawn side outside the plasmapause.
- The modeled propagation of wave characteristics depends strongly on the distribution of the warm (superthermal) electrons.
- Warm electrons play an important role in radiation belt dynamics, by controlling the chorus.

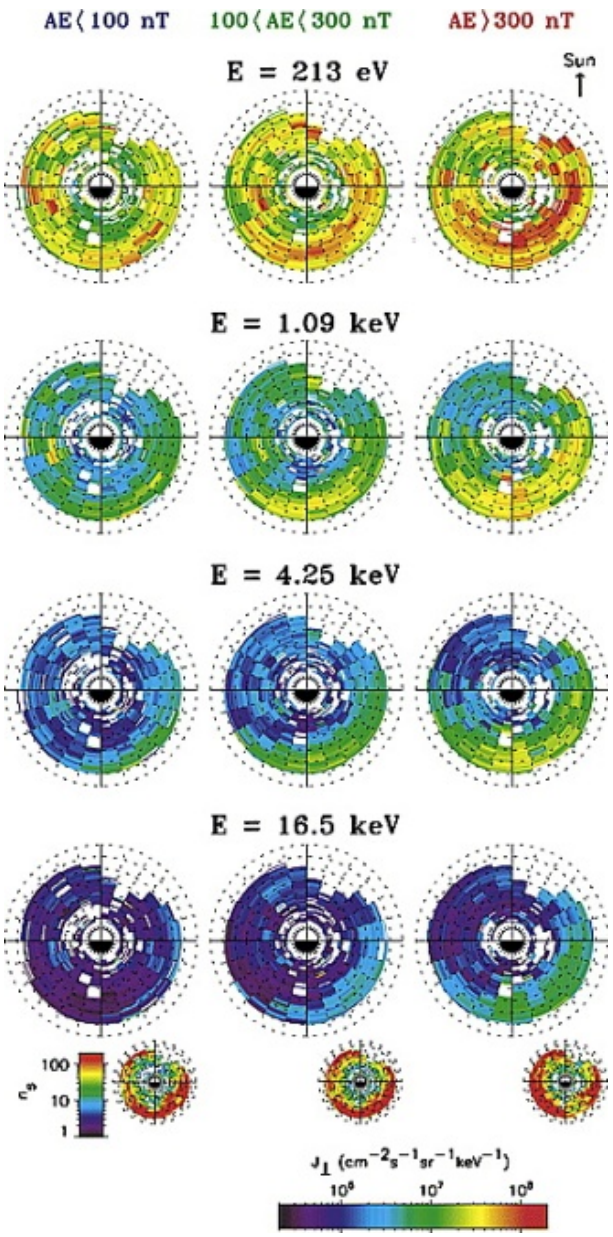

Average suprathermal electron fluxes measured with the LEPA instrument on the CRRES satellite. Distributions are shown as a function of L-shell and MLT, parameterized by energy (rows: 0.213, 1.09, 4.25, and 16.5 keV), and magnetic activity levels (columns: AE < 100 nT, 100 < AE < 300 nT, and AE > 300 nT). The common colorbar is shown at the bottom of the figure, together with the number of samples in each L-MLT bin.

Bortnik et al. (2007, JGR)

Ring current

What causes main phase Dst?

- Dst index is well anticorrelated with I_{vs}, where

$$I_{vs} = \int E_{vs}\, dt$$

E_{vs} is the electric field in the equatorial plane calculated combining the Volland-Stern and Siscoe-Hill model (Burke et al., 2007, JGR).

  - Penetration electric field drives main phase Dst.

- Main phase during northward IMF (Du et al., 2007, JGR)

  - Dst decreased when IMF is northward probably due to a delayed energy injection.

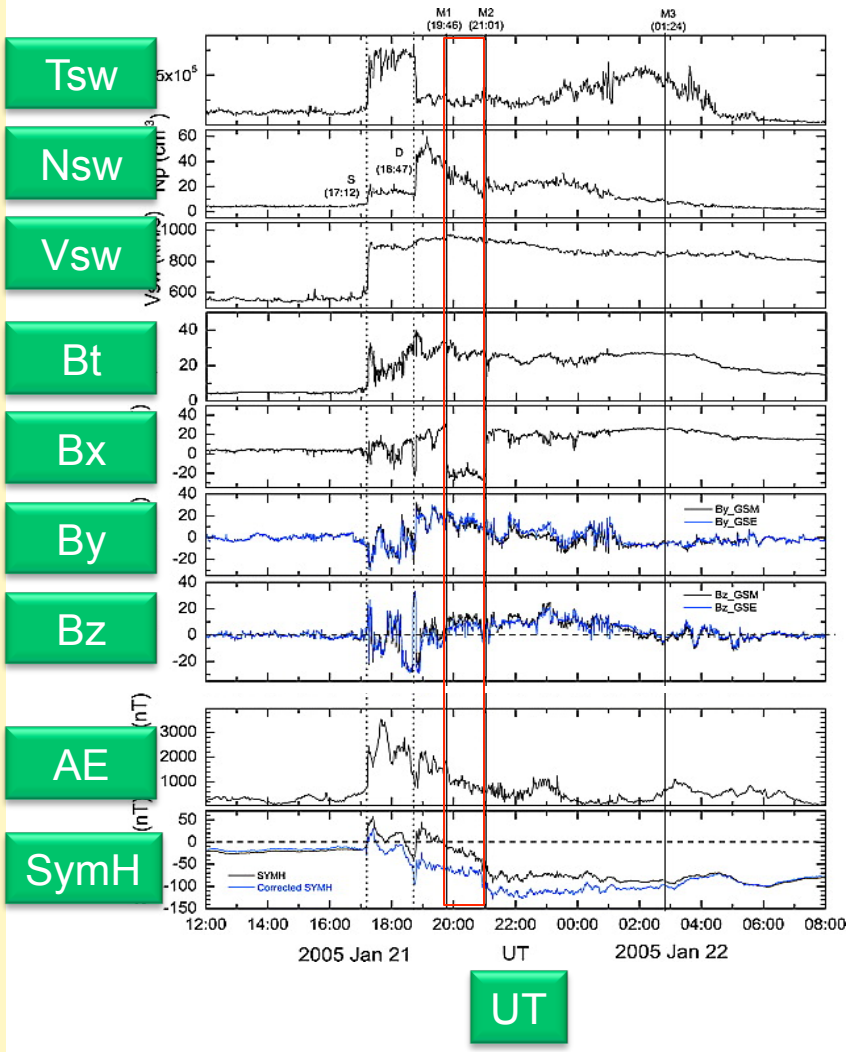

Du et al. (2007, JGR)

Mass driver for strong ring current

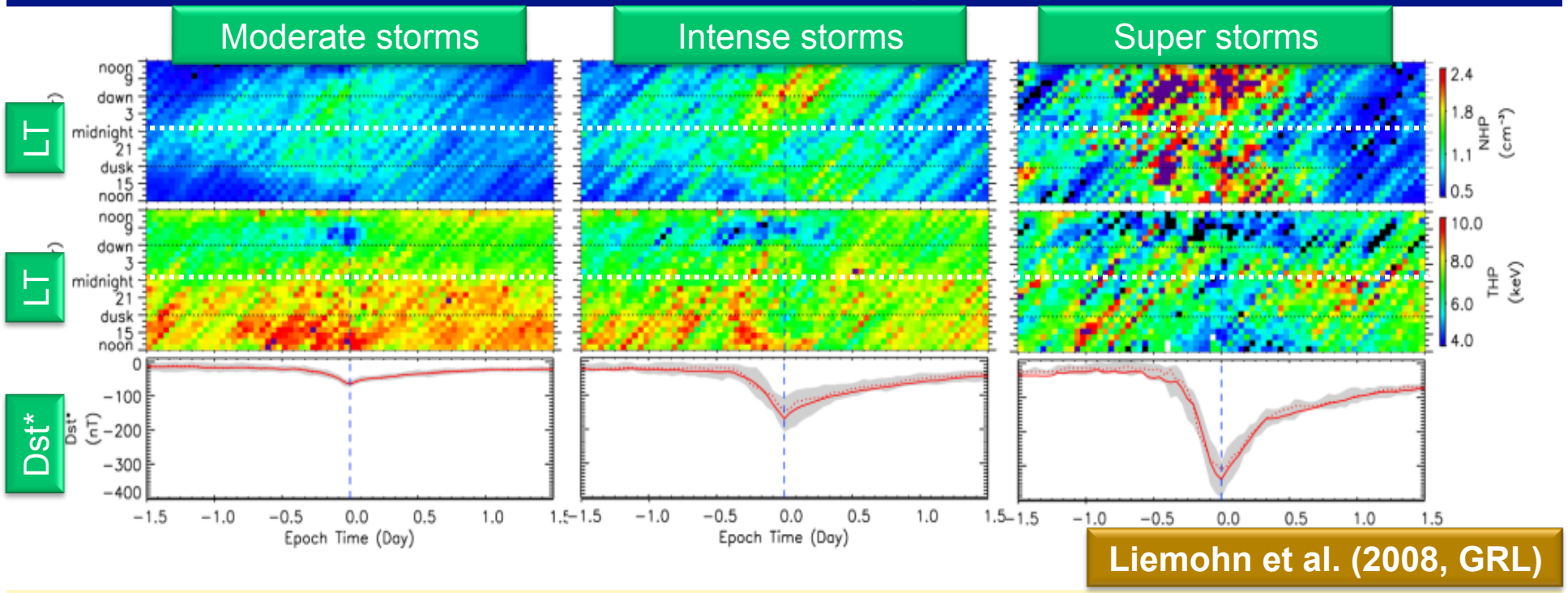

Liemohn et al. (2008, GRL)

- Plasma sheet ions are known to be a “mass” driver of the ring current.
- Superposed epoch analysis shows (Liemohn et al., 2008, GRL):
  - A systematic temperature drop in the post-dawn sector.
  - A systematic density enhancement in the post-dawn sector.
  - During super-storm, two density peaks 9 hours before the storm peak, and at the storm peak.
- Substantially large total energy to the ring current is provided from post-midnight sector (Lavraud et al., 2008, JGR).

Superdense plasma sheet caused by high-speed stream

- For 124 high-speed-stream driven storms:
  - The onset of the superdense plasma sheet in the magnetosphere is prior to storm onset.
  - The superdense ion plasma sheet and the superdense electron plasma sheet do not commence simultaneously.
  - The extra-hot plasma sheet commences with storm onset and persists for several days during the storm.

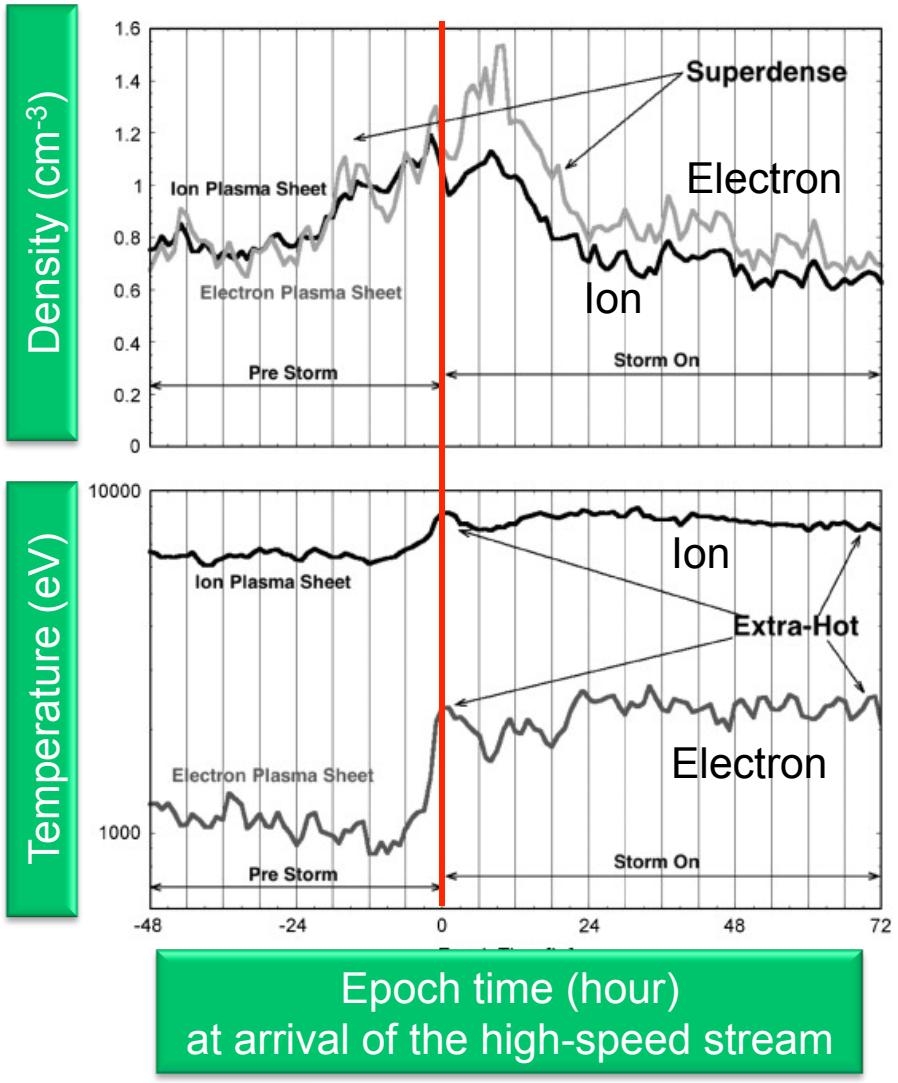

Denton and Borovsky (2009, JASTP)

Why doesn't RC injection rate saturate?

- Polar cap potential is known to be saturated for high solar wind electric field. But, the ring current intensity does not show saturation.
- Neutral line moves closer to the Earth, the volume per unit magnetic flux in the closed field line region is less.
- Flux tubes leaving the reconnection region have lower PV^{γ} as B_s increases.
- Lower PV^{γ} flux tubes can penetrate deeper into the inner magnetosphere, leading to a corresponding greater injection of particles into the inner magnetosphere.
- Thus a reconnection region that is closer to Earth is more effective in creating a strong ring current.

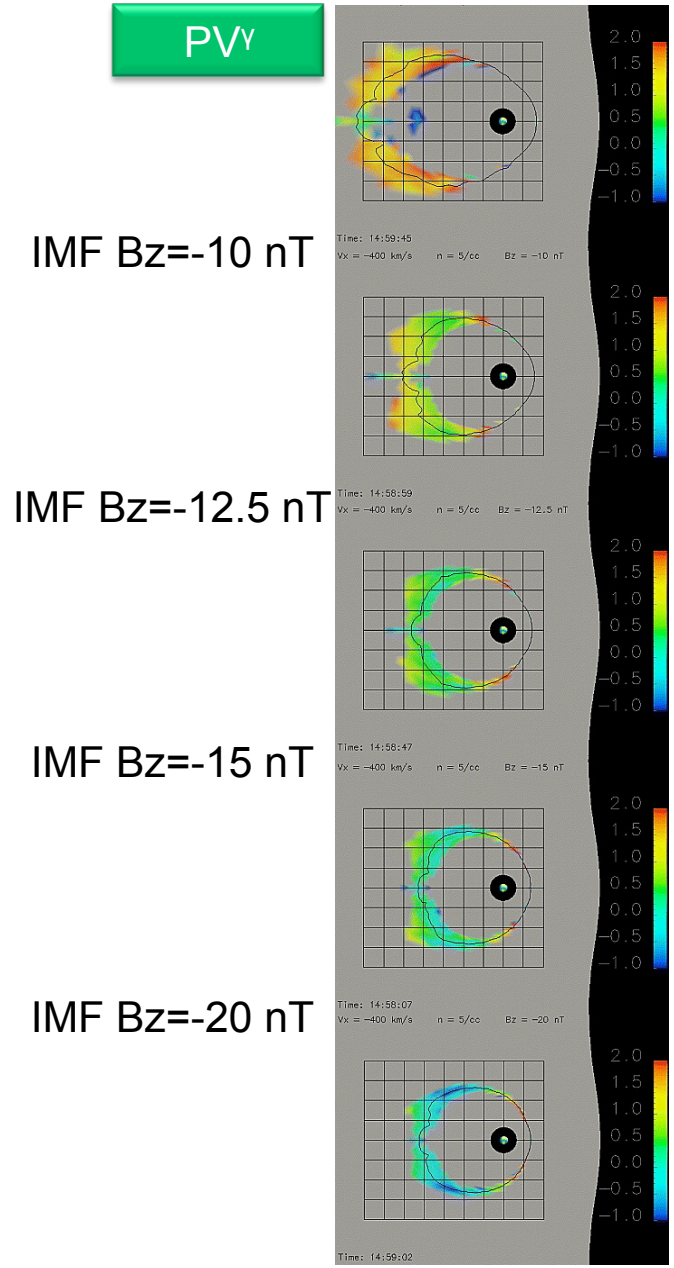

Lopez et al. (2009, JGR)

Oxygen ions in the ring current

- Multiple-banded structure of O^+ is found in the ring current, which may be an indication of a direct entry of O+ into the ring current (Yao et al., 2008, JGR).
- Oxygen ions are nonadiabatically accelerated by electric fields induced by the fluctuation of magnetic field (near gyrofrequency) during the dipolarization events (Ono et al., 2009, JGR).
- Not only low-charge-state O ions, but also high-charge-state O ions are almost simultaneously enhanced in the ring current during the storm times (Ebihara et al., 2009, JGR).

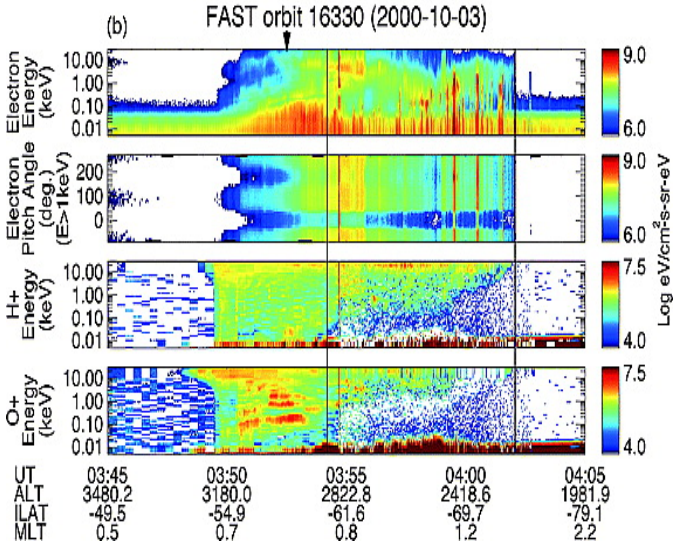

Yao et al. (2008, JGR)

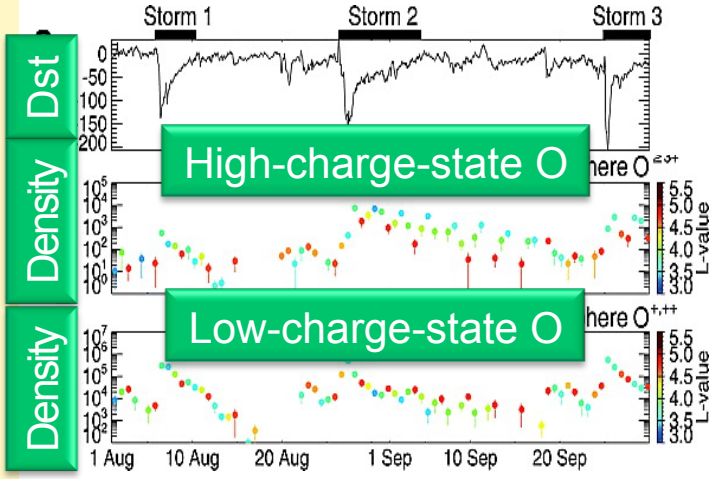

Ebihara et al. (2009, JGR)

Shocked ring current

- ENA flux (10-200 keV) was enhanced due to arrival of interplanetary shock (Lee et al., 2007, JGR).
  - For northward IMF without a substorm, interplanetary shock results in increase in the total ENA emission by 25 – 40 % due to adiabatic acceleration.
  - For southward IMF with a substorm, interplanetary shock results in increase in the total ENA emission by 100 %.
- Hot ion injection was found at dawn at GEO due to interplanetary shock (Han et al., JASTP, 2008).

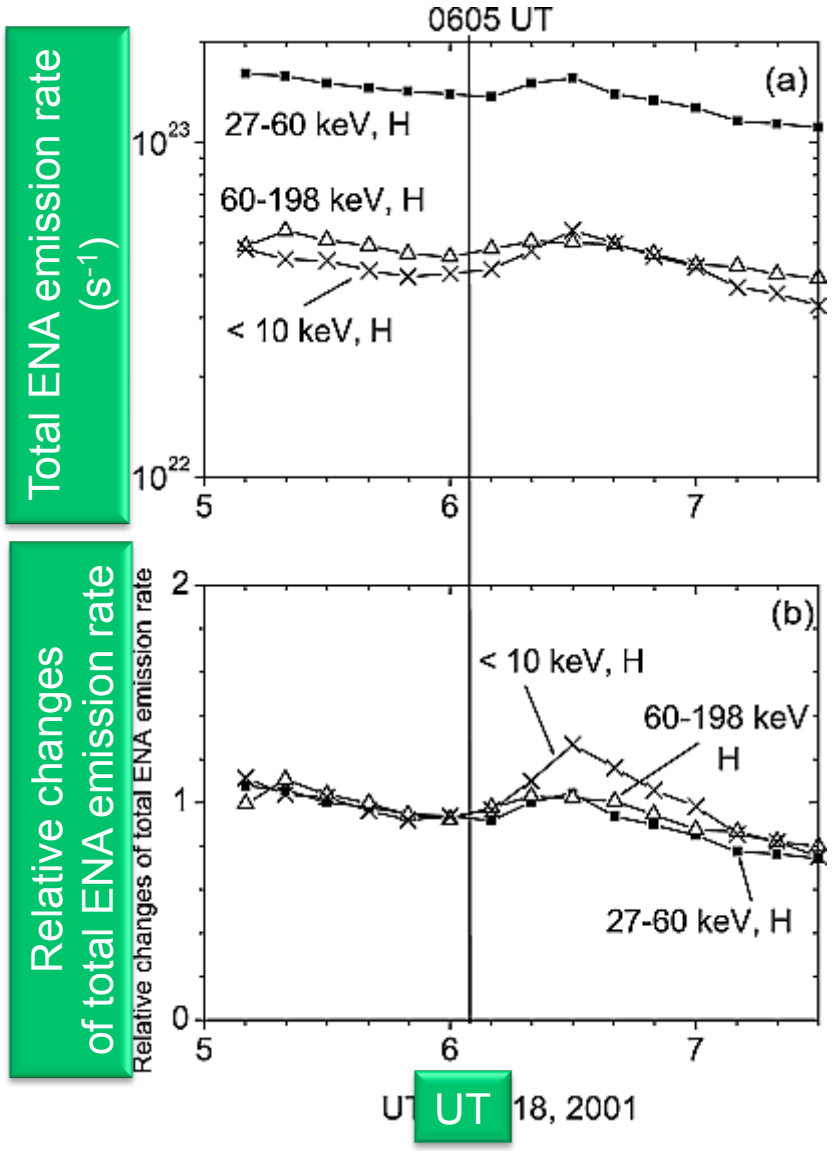

Lee et al. (2007, JGR)

Numerical treatment of the inner magnetosphere

- Ring current solved with “fluid treatment” is completely different from that solved with “kinetic treatment” (Song et al., 2008, JGR).
- Field-aligned current solved with non-force-balanced B-field is different from that solved with force-balanced one (Zaharia, 2008, JGR).

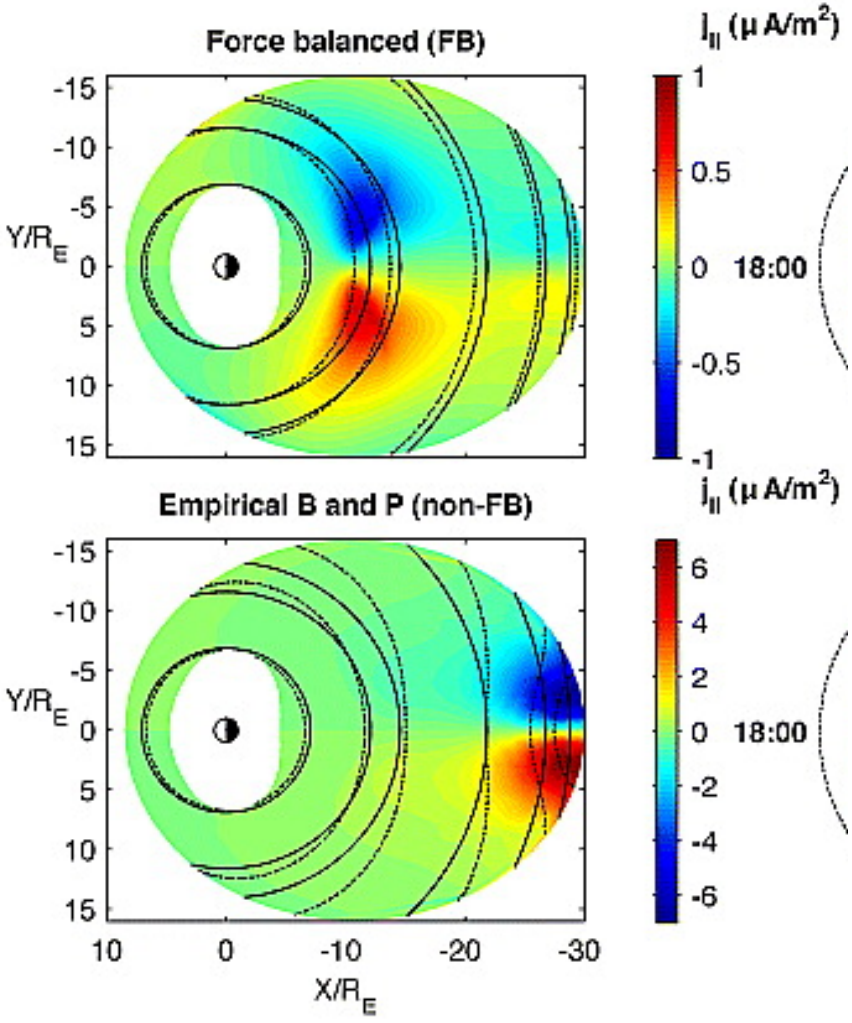

Zaharia (2008, JGR)

Radiation belt

Formation of ultrarelativistic (>10 MeV) electron

- There are three known cases where ultrarelativistic (>10 MeV) electrons appeared in the Earth's inner zone radiation belts.
  - March 1991, February 1994, October 2003.
- MHD model SC electric field pulse energizes the electron to 15 MeV.
- The newly formed belt is predominantly equatorially mirroring.
- Quasi-linear pitch angle diffusion accounts for the observed delay in the appearance of peak fluxes at SAMPEX in low Earth orbit .

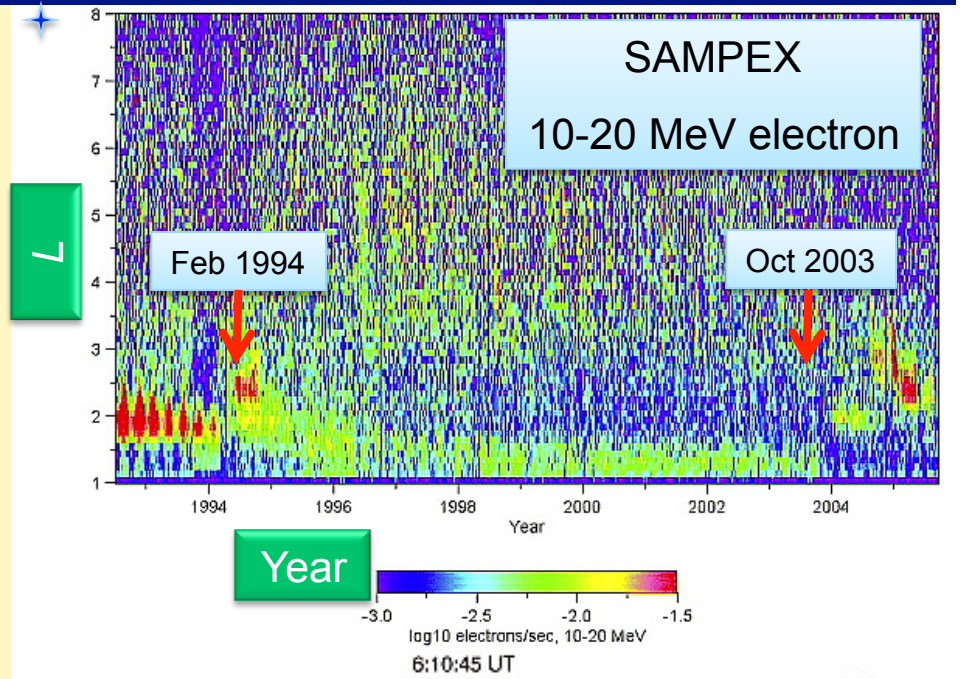

Daily averages of 10–20 MeV electron count rates from SAMPEX 1992 through 2005. A new belt injected during the 29 October 2003 storm appears as a weak enhancement near L = 2 beginning ~ February 2004.

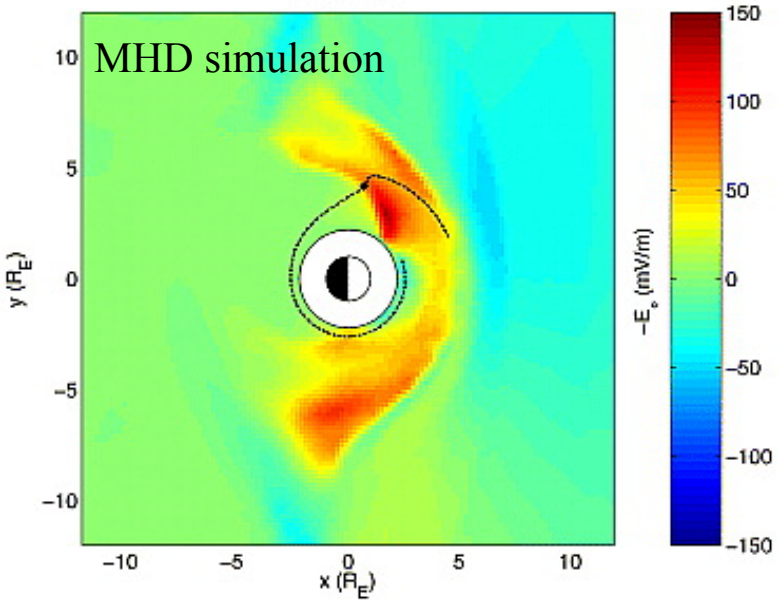

Snapshot of the azimuthal component of the MHD model SSC electric field pulse in the equatorial plane. The dashed line shows the trajectory of a single adiabatically accelerated guiding center electron in drift resonance with the pulse as it propagates from the dayside to nightside. The initial and final energies of the particle are ~5 and 15 MeV, respectively.

Kress et al. (2007, JGR)

Drift loss to magnetopause

- When the solar wind dynamic pressure increases, the equatorial omnidirectional flux of 1 MeV electrons at midnight near geosynchronous altitude decreases by ~56 to ~97%, depending on the specific pitch angle distribution of the directional flux (Kim et al., 2008).
  - The most significant loss of the 1 MeV electron flux takes place around L=7.
- Drift shell bifurcation violates the 2nd invariant. Radial diffusion coefficient (D_{LL}) and pitch angle diffusion coefficient ($D_{\alpha\alpha}$) for this process are formulated (Öztürk and Wolf, 2007, JGR).

Examples electron guiding center orbits in the T02 model. (a) Three types of drift paths. (b) Pitch angle-dependent drift shell.

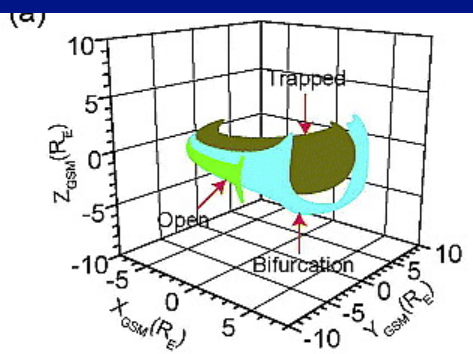

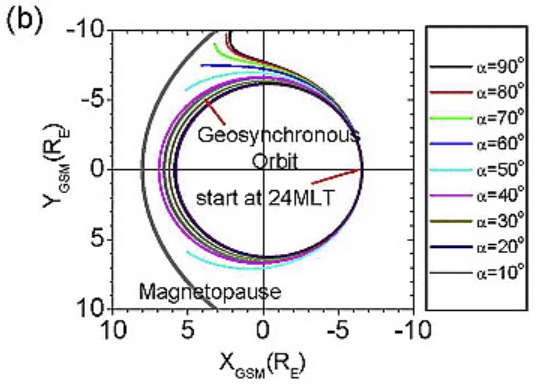

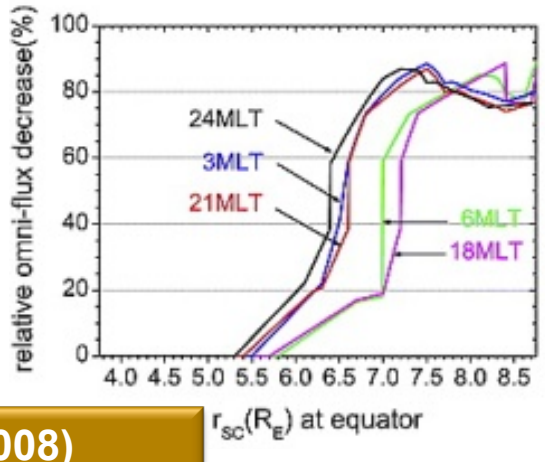

Kim et al. (2008)

What causes generation of strong MeV electron flux?

- For the generation of the strong MeV electron fluxes, the combination of two factors is needed (Lyatsky and Khazanov, 2008, JGR):
  - (1) strong geomagnetic disturbances, and
  - (2) low solar wind density

  about 2 days before the following increases in electron fluxes.
- The growth rate of the ion/electron-cyclotron waves increases with decreasing the Alfven velocity, which is inversely proportional to the square root of the plasma density. Penetrating the solar wind plasma into the inner magnetosphere makes an important factor affecting the losses of relativistic electrons.

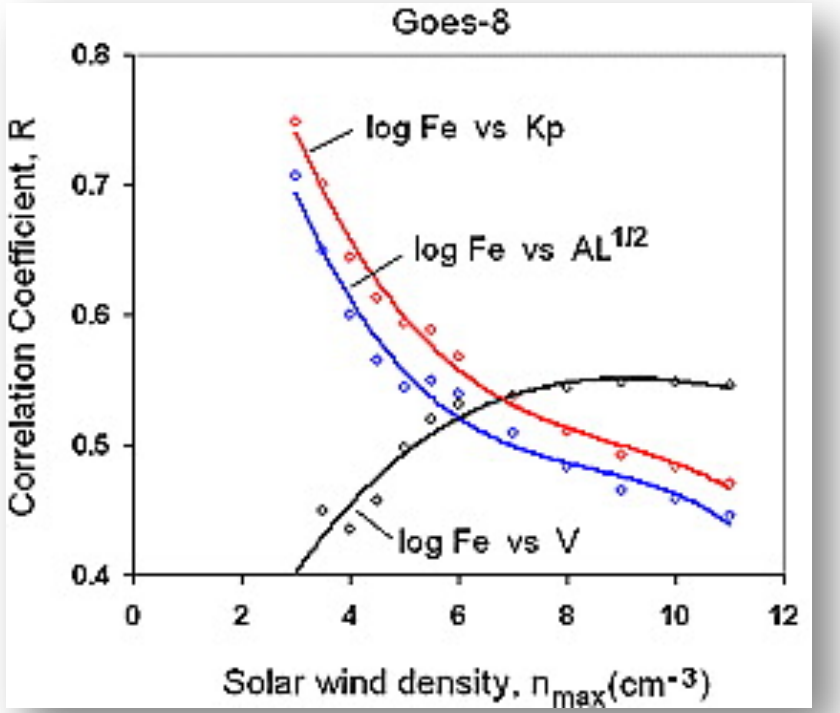

(Black) Correlation coefficients between electron flux and the solar wind velocity as a function of the solar wind density. The correlation coefficient is high for dense solar wind. They obtained higher correlation coefficients between electron flux and the Kp index (red), and the square root of the AL index (blue).

Lyatsky and Khazanov (2008, JGR)

Storm-time PSD peak confirmed

- Phase space density (PSD) at constant 1st and 2nd invariants provide a test of whether storm time electron acceleration process dominates inward radial transport of electrons.
- Data from SCATHA show that PSD has peaks in L=5.2-6.5 for intermediate to large K in the storm recovery phase (Fennell and Roeder, 2008, JASTP).

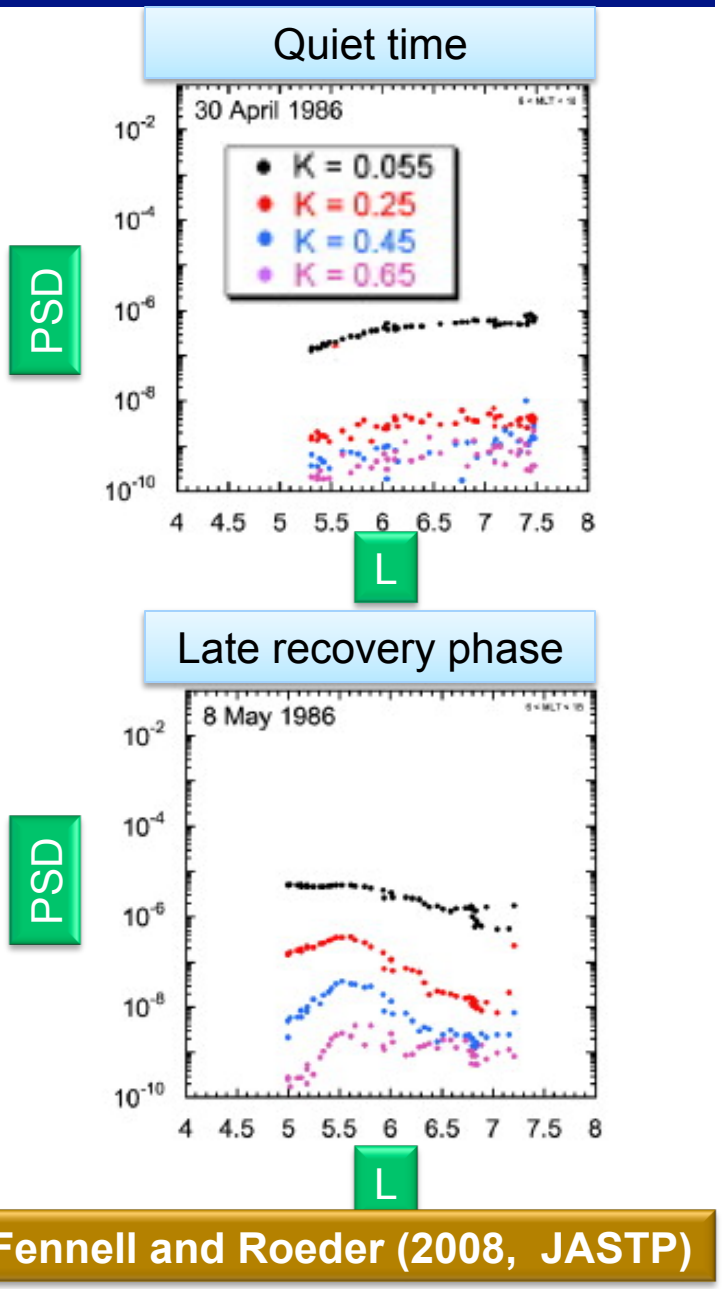

Relativistic electron stimulated by high-speed stream

- High-speed-stream results in abrupt enhancement of relativistic electrons (Miyoshi and Kataoka, JGR, 2008; Borovsky and Denton, JGR, 2009).
- Russel-McPherron effect plays a major role in energization processes of relativistic electrons (Miyoshi and Kataoka, 2008; McPherron et al., JASTP, 2009).

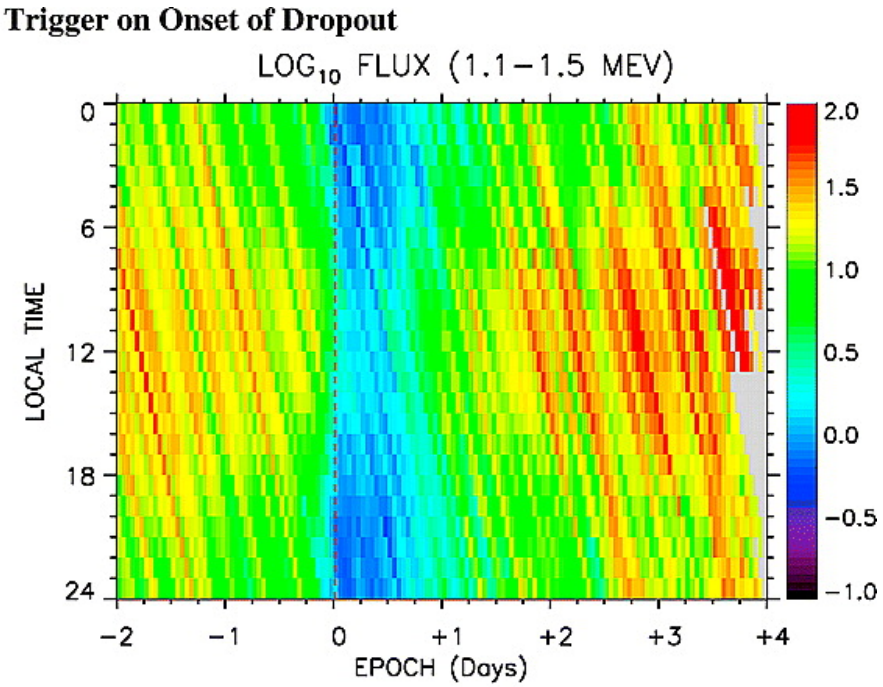

Borovsky and Denton (2009, JGR)

Logarithm of the flux of 1.1–1.5 MeV electrons around geosynchronous orbit is plotted for a set of 33 events with clear onsets to relativistic-electron dropouts, with the triggering of the superposition being the onset of dropout. (bottom) Logarithm of the flux of 1.1–1.5 MeV electrons around geosynchronous orbit is plotted for a set of 14 events with clear recoveries to relativistic-electron dropouts, with the triggering of the superposition being the recovery from dropout.

CIR vs. magnetic activity and relativistic electrons

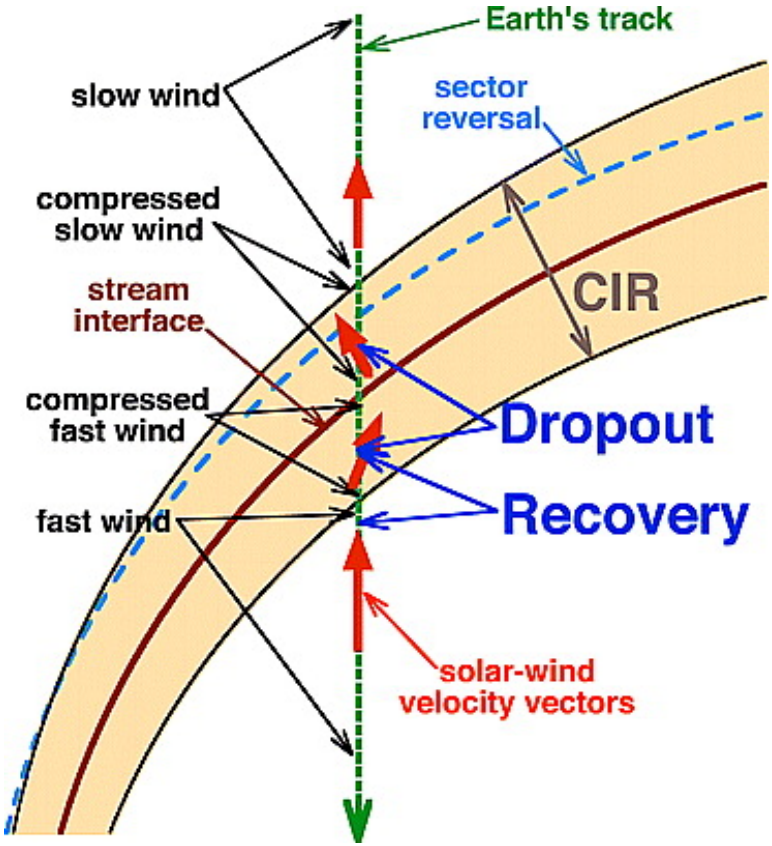

Looking down onto the ecliptic plane from above, a CIR near Earth's orbit is sketched. The Sun is off the bottom of the figure. The CIR is shaded in tan, and the Earth's track through the CIR is depicted as the green dashed line. In the reference frame of this sketch, the Earth moves downward with time. The solar wind flow direction is shown with red arrows. At first, the Earth is in the slow wind ahead of the CIR. As the Earth enters the CIR, it enters into compressed slow wind with a flow deflection to the left. When the Earth crosses the stream interface (dark red), it exits the compressed slow wind and enters the compressed fast wind and the flow deflection switches from left to right. When the Earth exits the CIR, it exits into fast wind with no flow deflection. Typically, ahead of the stream interface, there is a magnetic-field sector reversal (light-blue dashed curve) where the field switches from inward to outward or from outward to inward. In dark blue, the positions of the Earth on its track where the relativistic-electron dropout and recovery from dropout occur are indicated. (See Table 1 for details.)

Solar Wind at Earth	Stage of Geomagnetic Activity	Relativistic-Electron-Dropout Status
Slow wind	Calm occurs ~70% of time	Relativistic-electron flux slow decay
CIR starts	Calm ends	Relativistic-electron flux slow decay
Compressed slow wind (westward flow)	Mild geomagnetic activity	Relativistic-electron flux slow decay
Sector reversal in compressed slow wind	Geomagnetic activity rises	Relativistic-electron flux slow decay
Compressed slow wind with southward IMF	Storm onset	Onset of dropout
Stream interface (flow reversal)	Storm levels	Dropout ongoing
Compressed fast wind (eastward flow)	Storm levels	Recovery of dropout commences
CIR ends	Storm levels	Recovery progressing
Fast wind	Activity slowly declines	Recovery complete

Borovsky and Denton (2009, JGR)

Physical models of relativistic electrons

- RADICAL (Lam et al., 2007, GRL)
  - 1D (1D in space).
  - Boundary given by CRRES observation.
  - D_{LL} depending on Kp.
  - $D_{\alpha\alpha}$ for Hiss.
- Salammbô (Maget et al., 2007, Space Weather)
  - 3D (1D in space, 2D in velocity space).
  - Boundary given by observation at GEO.
  - $D_{\alpha\alpha}$, D_{EE} for Hiss and whistler mode chorus.
  - Empirical plasmaspheric model.
- RBE (Fok et al., 2008, JGR)
  - 4D (2D in space, 2D in velocity space).
  - Boundary given by empirical model driven by solar wind.
  - $D_{\alpha\alpha}$, D_{EE} for whistler mode chorus.
  - Physical plasmaspheric model.

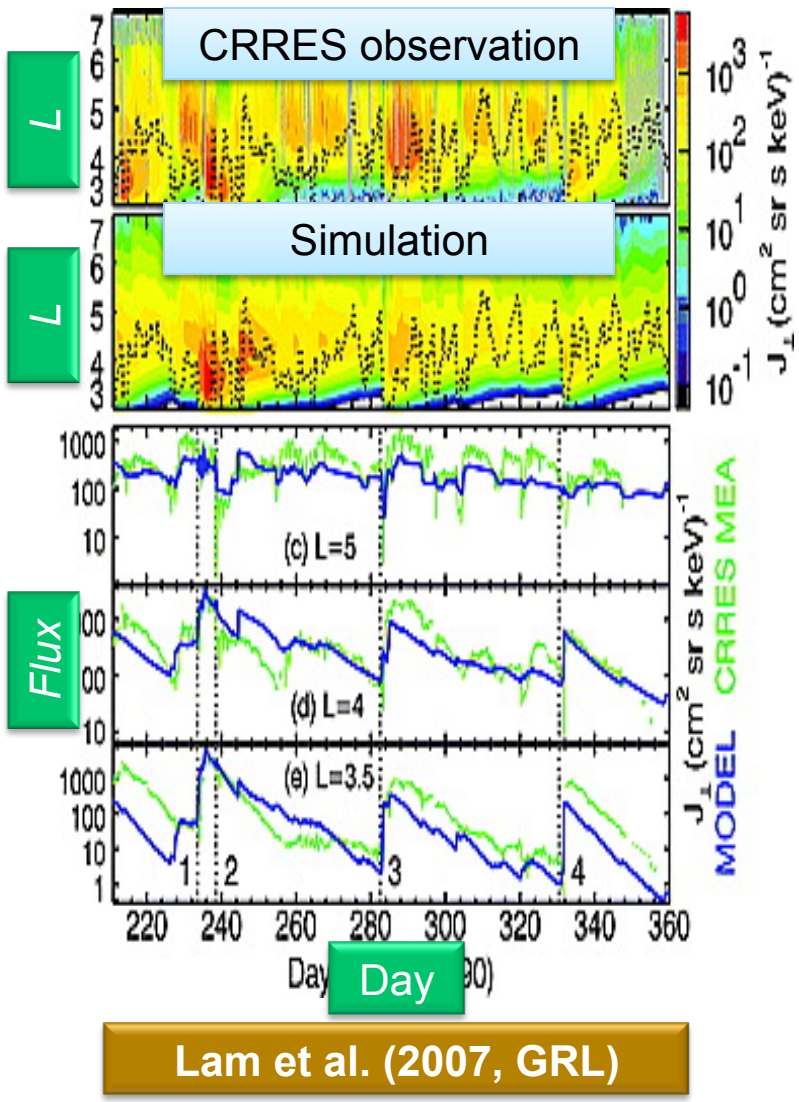

They find that during magnetic storms hiss can cause significant losses for $L \leq 6$ due to its presence in plumes.

Physical models of relativistic electrons

- RADICAL (Lam et al., 2007, GRL)
  - 1D (1D in space).
  - Boundary given by CRRES observation.
  - D_{LL} depending on Kp.
  - $D_{\alpha\alpha}$ for Hiss.
- Salammbô (Maget et al., 2007, Space Weather)
  - 3D (1D in space, 2D in velocity space).
  - Boundary given by observation at GEO.
  - $D_{\alpha\alpha}$, D_{EE} for Hiss and whistler mode chorus.
  - Empirical plasmaspheric model.
- RBE (Fok et al., 2008, JGR)
  - 4D (2D in space, 2D in velocity space).
  - Boundary given by empirical model driven by solar wind.
  - $D_{\alpha\alpha}$, D_{EE} for whistler mode chorus.
  - Physical plasmaspheric model.

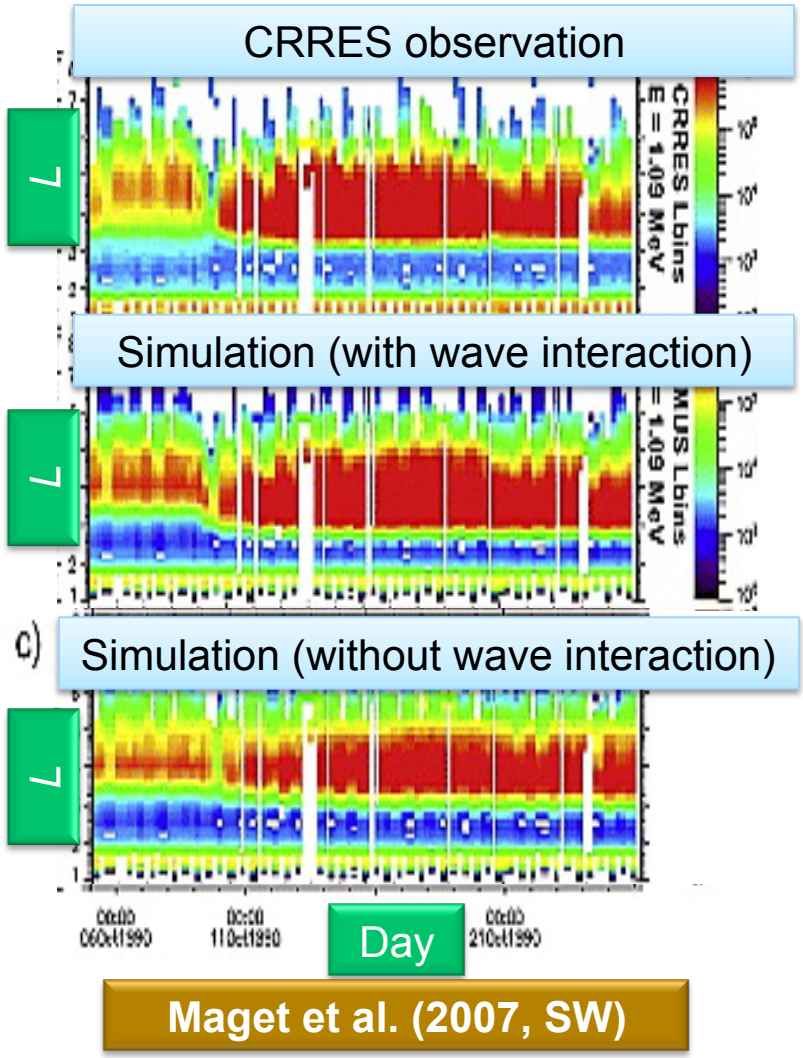

Physical models of relativistic electrons

- RADICAL (Lam et al., 2007, GRL)
  - 1D (1D in space).
  - Boundary given by CRRES observation.
  - D_{LL} depending on Kp.
  - $D_{\alpha\alpha}$ for Hiss.
- Salammbô (Maget et al., 2007, Space Weather)
  - 3D (1D in space, 2D in velocity space).
  - Boundary given by observation at GEO.
  - $D_{\alpha\alpha}$, D_{EE} for Hiss and whistler mode chorus.
  - Empirical plasmaspheric model.
- RBE (Fok et al., 2008, JGR)
  - 4D (2D in space, 2D in velocity space).
  - Boundary given by empirical model driven by solar wind.
  - $D_{\alpha\alpha}$, D_{EE} for whistler mode chorus.
  - Physical plasmaspheric model.

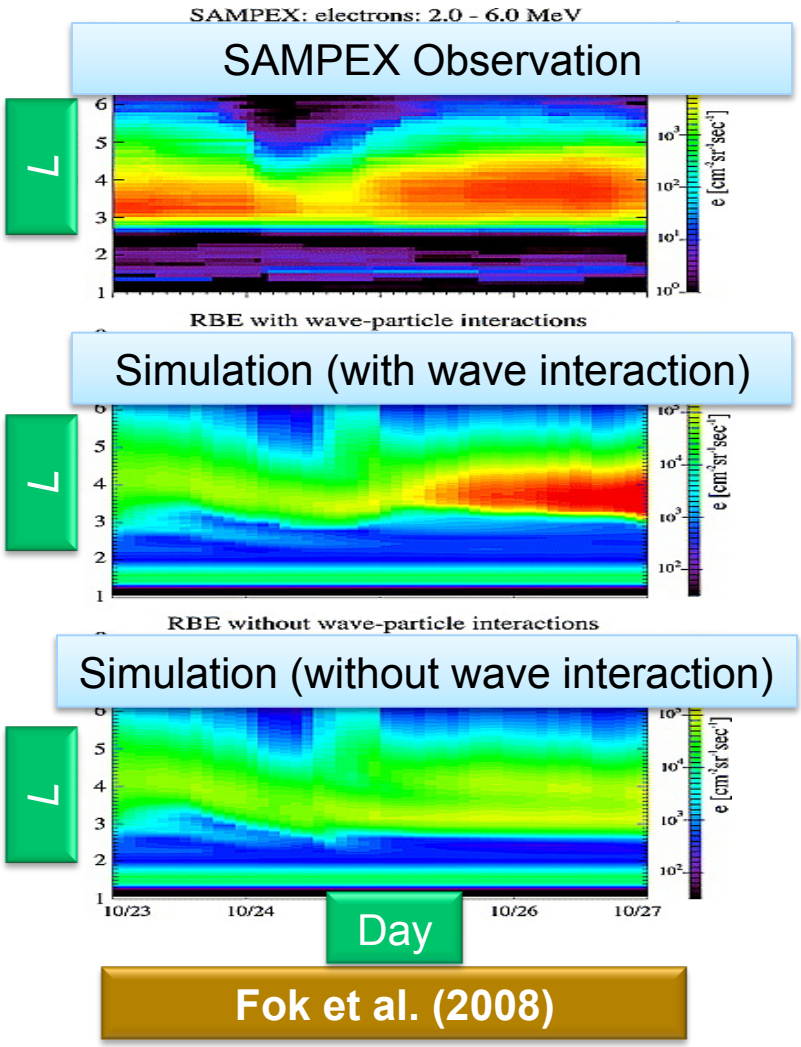

SAMPEX 2–6 MeV electron L-time diagram during the storm on 23–27 October 2002 and RBE simulated fluxes in T04 magnetic field (middle) with and (bottom) without inclusion of wave-particle interactions, respectively.

Physical models of relativistic electrons (cont.)

- Degeling et al. (2008, JGR)
  - 3D (2D in space, 1D in velocity space).
  - Induction electric field due to ULF waves.
  - A burst of narrow band ULF waves can give rise to the growth of strong localized peaks in PSD with L-shell by nondiffusive radial transport.
- Tu et al. (2009, JGR)
  - 1D (1D in space).
  - D_{LL} depending on Kp.
  - τ for chorus, hiss, and EMIC waves.
  - Heating term (source term).
  - Boundary condition given by GPS.

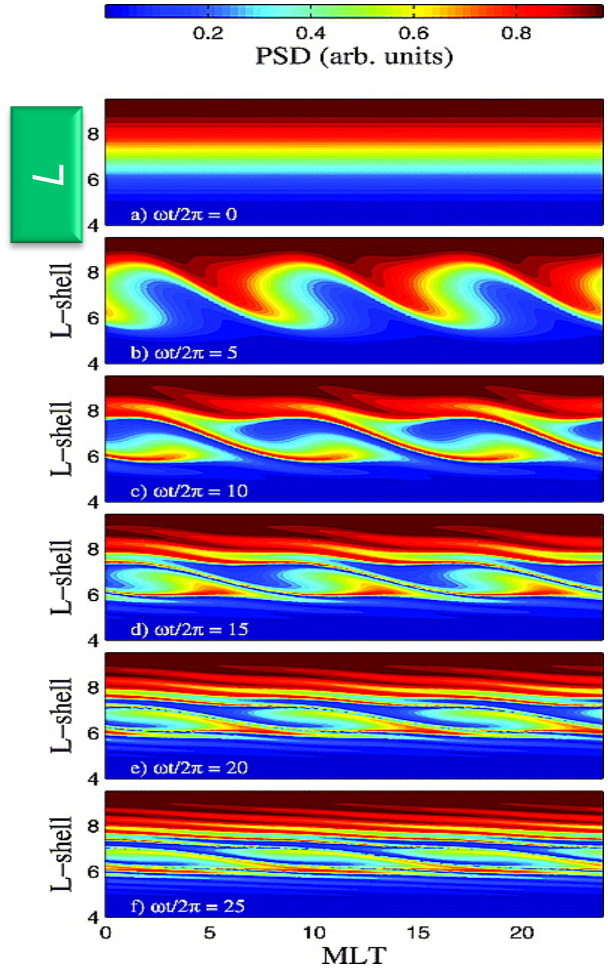

Degeling et al. (2008, JGR)

Contour plots of phase space density as functions of L-shell and MLT

Sawtooth events

Sawtooth event

- Average period of sawtooth event is 179.6 min, and is quasi-periodic, NOT periodic (Cai and Clauer, 2009, JGR).
- Quasi-periodic loading-unloading cycles made by MHD simulation causes enhanced ring current injection (Taktakishvili et al., 2007, JGR).
- Dipolarization and particle energization were found at 4.6 Re (Ohtani et al, 2007).
- Sawtooth causes interchange instability, and spatial quasi-periodic auroral arcs (Yang et al., 2008, JGR).

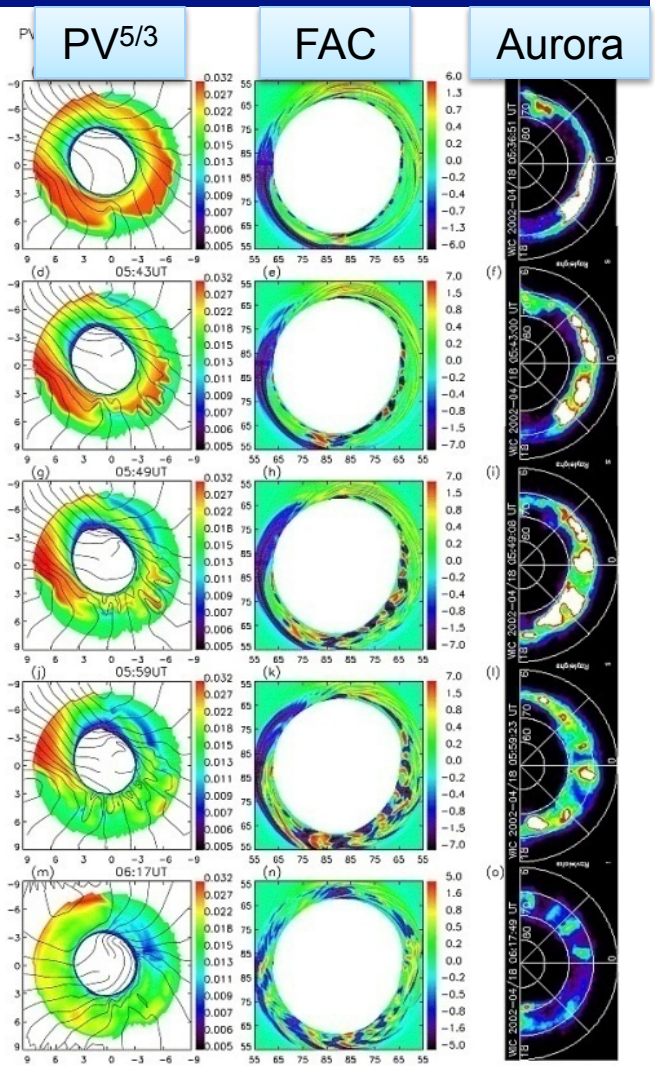

Yang et al. (2008, JGR)

Spatial quasi-periodic auroral arcs observed by an IMAGE/FUV WIC detector might be caused by interchange instability.

Ionosphere coupling: SAPS/SAID

Ionosphere coupling: SAPS/SAID

- SubAuroral Polarization Stream, SubAuroral Ion Drift, Polarization Jet, SubAuroral Electric Field, Drift Spike
- The latitude of SAPS channel varies directly with the magnitude of Dst (Huang and Foster, 2007, JGR)
  - Λ=57.6+0.04×Dst
  - SAPS is related to the ring current.
- Seasonal variation of SAPS was found (Wang et al., 2008).
  - There is a good correlation between the subauroral integrated conductivity and the SAPS latitude.
  - There is a good anticorrelation between the conductivity and the SAPS velocity.
- SAPS are frequently an important aspect of the inner magnetospheric electric field and magnetosphere-ionosphere coupling, including substorms (Lyons et al., 2008, JASTP).

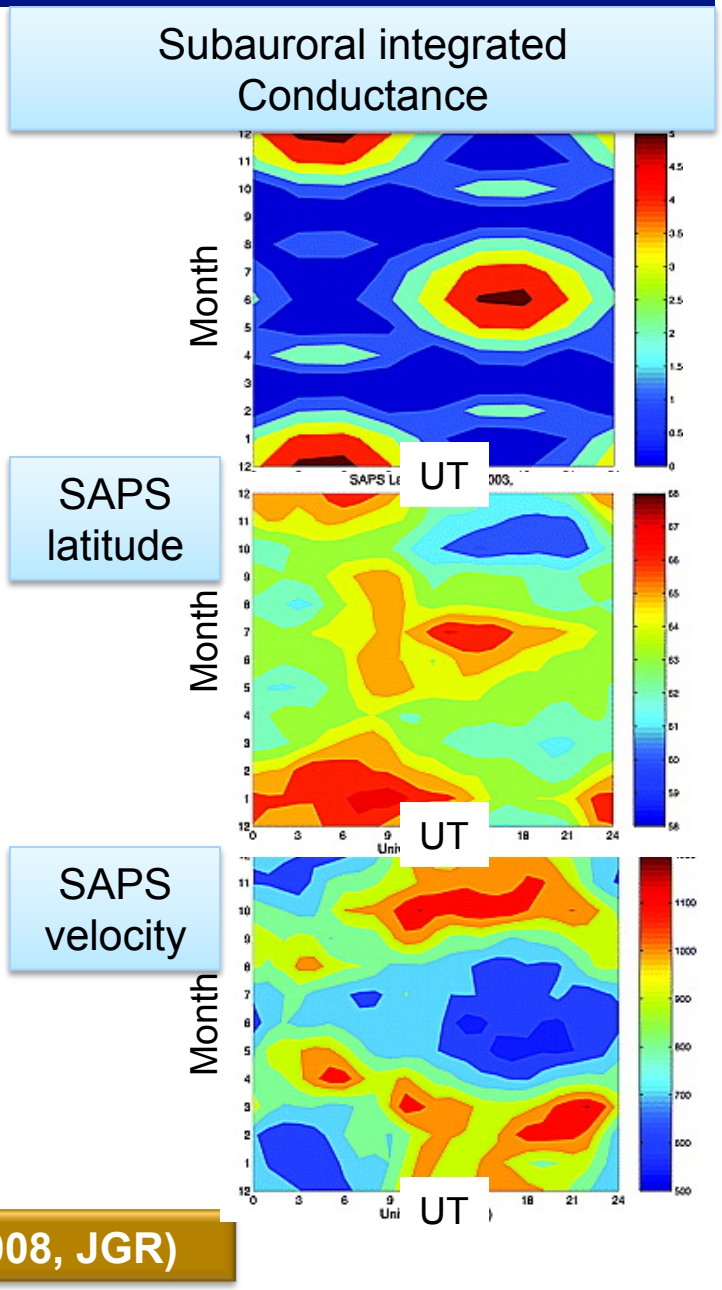

Wang et al. (2008, JGR)

Ionosphere coupling: Variety of SAPS/SAID

Mirror eastward flow channel

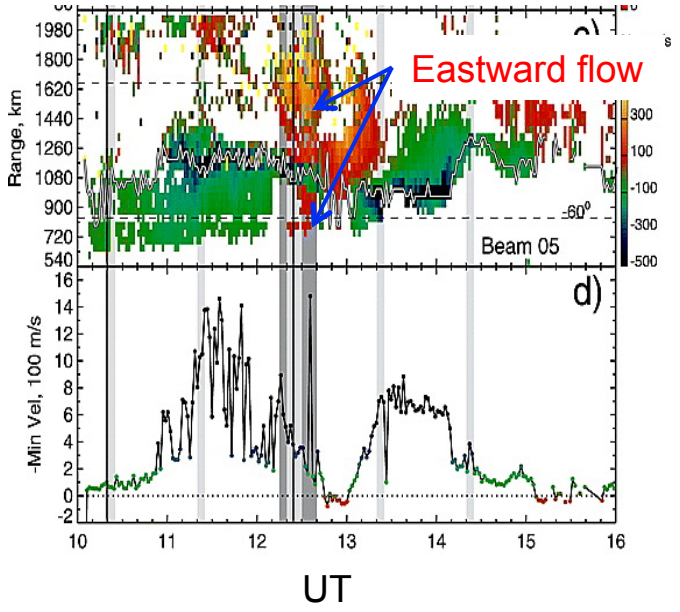

Makarevich et al. (2009, JGR)

Abnormal SAID (ASAID)

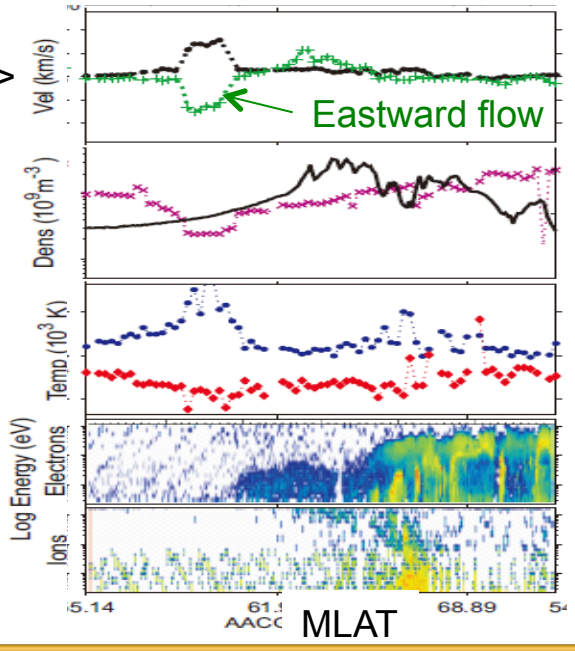

Voiculescu and Roth (2008, AG)

Temporal variation

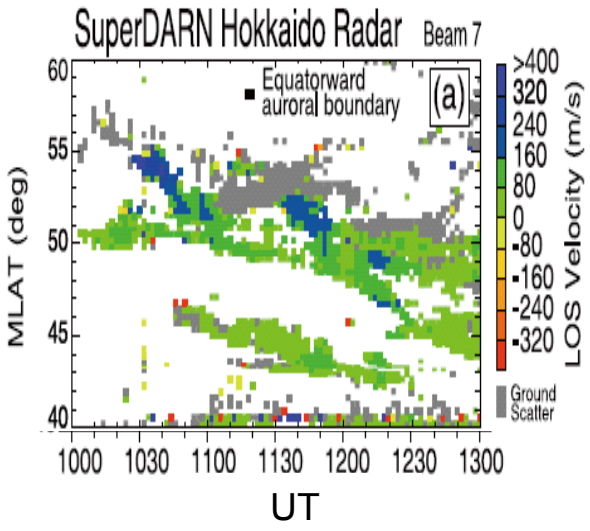

Ebihara et al. (2009, JGR)

- Westward SAPS is sandwiched by eastward flow (Makarevich et al., 2009, JGR).
- Eastward plasma flow (abnormal SAID) was found (Voiculescu and Roth, 2008, AG).
- Temporal variation of SAPS (~5-10 min.) was found (Ebihara et al., 2009, JGR).
- Convection flow reversal on the dawnside was found (Kataoka et al., 2007, GRL). Dawnside extension of SAPS?
- SAPS was developed just after a substrorm (~30 sec) (Nishimura et al., 2008, GRL).

Ionosphere coupling: Aurora

Shock-induced ring current aurora

- Protons precipitate into the subauroral ionosphere just after SC. Polar observed EMIC waves associated with the proton aurora. (Zhang et al., 2008, JGR).
- Spot-like proton aurora was found in conjunction with Pc1 activity on the ground (Yahnina et al., 2008, JGR).
- Kinetic simulation with EMIC waves explains the formation of the spot-like proton aurora on the dayside (Jordanova et al., 2007, JGR).
- Spot-like proton aurora and Pc1 activity were simultaneously observed in the subauroral region regardless of magnetic activity and solar wind condition (Sakaguchi et al., 2008, JGR).

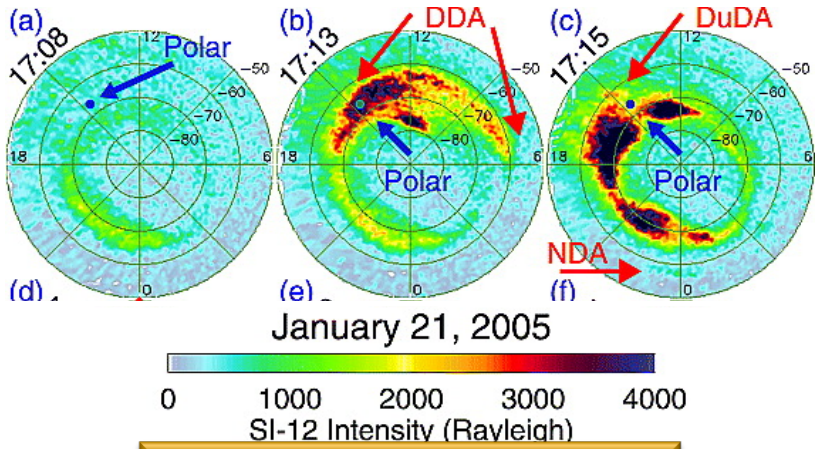

Zhang et al. (2008, JGR)

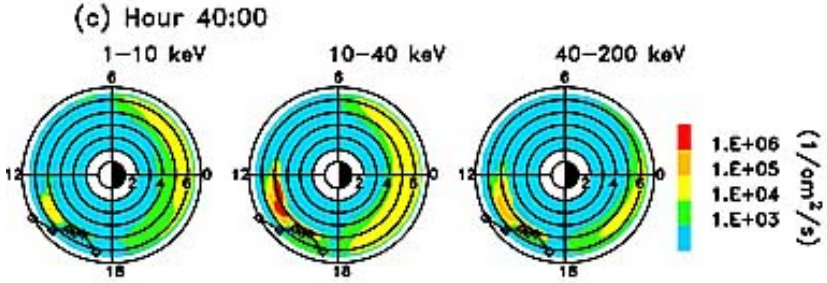

Jordanova et al. (2007, JGR)

Summary

- Significant progress is achieved in the last 2 years due to analysis of data from SCATHA, CRRES, SAMPEX, IMAGE, GEO satellites, and THEMIS as well as ground-based observation and numerical modeling.
- Plasmasphere, ring current, and the radiation belt are NOT independent from each other. Importance of inter-energy coupling has been well established.
- State of the inner magnetosphere depends largely on the solar wind condition and the ionosphere as well. Inter-region coupling should be taken into consideration.

Outstanding question

- Entry of solar wind plasma into the ring current is a key in understanding the ring current and the radiation belt.
- Overall influence of internal mass driver (e.g., plasmaspheric wind and outflowing of oxygen ions) on the magnetosheric dynamics is unknown.
- Each element constituting the inner magnetosphere has been investigated in detail. Question: What causes what?